Wobbling geometry in a simple triaxial rotor *

SHI Wen-Xian(施文娴)[1,2] CHEN Qi-Bo(陈启博)[1;1)]

[1] State Key Laboratory of Nuclear Physics and Technology, School of Physics, Peking University, Beijing 100871, China
[2] Yuanpei College, Peking University, Beijing 100871, China

Abstract: The spectroscopic properties and angular momentum geometry of the wobbling motion of a simple triaxial rotor are investigated within the triaxial rotor model. The obtained exact solutions of energy spectra and reduced quadrupole transition probabilities are compared to the approximate analytic solutions from the harmonic approximation formula and Holstein-Primakoff formula. It is found that the low lying wobbling bands can be well described by the analytic formulae. The evolution of the angular momentum geometry as well as the K-distribution with respect to the rotation and the wobbling phonon excitation are studied in detail. It is demonstrated that with the increase of the wobbling phonon number, the triaxial rotor changes its wobbling motions along the axis with the largest moment of inertia to the axis with the smallest moment of inertia. In this process, a specific evolutionary track that can be used to depict the motion of a triaxial rotating nucleus is proposed.

Key words: wobbling motion, angular momentum geometry, triaxial rotor model

PACS: 21.60.Ev, 21.10.Re, 23.20.Lv **DOI:** 10.1088/1674-1137/39/5/054105

1 Introduction

The concept of wobbling motion was originally proposed more than forty years ago by Bohr and Mottelson when they investigated the rotational modes for a triaxial nucleus using a triaxial rotor model (TRM) [1]. In that pioneering work, they pointed out that the rotational angular momentum for a triaxial nucleus is not aligned along any of the body-fixed axes, but precesses and wobbles around the axis with the largest moment of inertia (MOI). The wobbling mode arises from the rotation of the triaxial nucleus along the axis with the largest MOI being quantum mechanically disturbed by the rotations along the other two axes. This is due to the fact that the loss of axial symmetry for a triaxial nucleus leads to the MOIs for the three axes being different from each other and thus makes rotations along all three axes possible. Therefore, the wobbling motion is regarded as a specific characteristic of a triaxial deformed nucleus, and together with chiral symmetry breaking [2–4], is considered as a unique fingerprint associated with the stable triaxial shape in nuclei.

The corresponding energy spectra for the wobbling mode are wobbling bands, a sequence of $\Delta I = 2$ rotational bands that build on different wobbling phonon excitations [1]. These kinds of bands were first observed in the odd-A nucleus ^{163}Lu [5] and soon after were identified in the triaxial strongly deformed region around $N = 94$ in ^{161,163,165,167}Lu [6–11] and ^{167}Ta [12]. For even-even nuclei, the best example identified so far is ^{112}Ru [13].

On the theoretical side, the wobbling motion has been studied with the TRM [1] and particle rotor model (PRM) [14–16], both of which are quantal models and exactly solved in the laboratory frame. Based on the framework of the cranking mean field theory, the random phase approximation method [17–24], the generator coordinate method after angular momentum projection (GCM+AMP) [25], and the collective Hamiltonian [26] have been employed for investigating the wobbling motion. In addition, some approximate analytic solutions, such as the harmonic approximation (HA) formula [1, 16] and Holstein-Primakoff (HP) formula [27–29], were also obtained to describe the energy spectra and electromagnetic transition probabilities of the wobbling motion.

Besides the energy spectra and electromagnetic transition probabilities, it would be very interesting to study the angular momentum geometry pictures of the wobbling motions. In Refs. [6, 7, 14], the angular momentum

Received 17 November 2014

∗ Supported by President's Undergraduate Research Fellowship (PURF), Peking University, Major State 973 Program of China (2013CB834400), National Natural Science Foundation of China (11175002, 11335002, 11375015, 11345004, 11461141002), National Fund for Fostering Talents of Basic Science (NFFTBS) (J1103206) and Research Fund for the Doctoral Program of Higher Education (20110001110087)

1) E-mail: qbchen@pku.edu.cn

components as functions of spin for low lying wobbling bands are analyzed with the PRM to study the nature of many-phonon wobbling excitations. Undoubtedly, such investigations of the angular momentum geometry are essential to deeply understand the picture of wobbling motion. However, to our knowledge, such investigations are still rather rare. Therefore, it is imperative to systematically study the angular momentum geometry of wobbling motion.

In this paper, for simplicity, a simple triaxial rotor is taken as an example to study the angular momentum geometry of wobbling motion by the TRM. The energy spectra and reduced quadrupole transition probabilities are obtained by exactly solving the TRM Hamiltonian and are compared with those approximate analytical results obtained by the HA [1] and HP [27] methods to evaluate the accuracy of the approximations. The geometry of angular momentum as well as the K-distribution will be analyzed in detail as functions not only of spin but also of wobbling phonon number.

The paper is organized as follows. In Section 2, the procedures for exactly and approximately solving the TRM Hamiltonian are presented briefly. The corresponding numerical details used in the calculations are given in Section 3. In Section 4, the energy spectra and reduced quadrupole transition probabilities obtained by exactly solving the TRM are shown and compared with those approximate results from the HA and HP methods. The angular momentum components and K-distribution evolution pictures as functions of spin and wobbling phonon number are investigated. Finally, a brief summary is given in Section 5.

2 Theoretical framework

2.1 Triaxial rotor model

The triaxial rotor model was firstly introduced for the description of a rotating triaxial nucleus by Davydov and Filippov [30] with the assumption that the nucleus has a well-defined potential minimum at a nonzero value of triaxial deformation parameter γ. Due to the anisotropy of a triaxial rotor, the nucleus can rotate around any of the principal axes. The corresponding Hamiltonian thus reads as

$$\hat{H}=A_1\hat{I}_1^2+A_2\hat{I}_2^2+A_3\hat{I}_3^2, \tag{1}$$

in which A_k are related to the MOIs of the three principal axes $\mathcal{J}_k$ by $A_k=\dfrac{\hbar^2}{2\mathcal{J}_k}$, $k=1,2,3$. The details for exactly solving this Hamiltonian by diagonalization can be found in Ref. [30] or in classical textbooks, e.g. Ref. [31]. In this subsection, for completeness, a brief introduction is presented.

The TRM Hamiltonian (1) is invariant under 180° rotation about the intrinsic principal axes (D_2 symmetry group). Thus the basis states $|IMK\alpha\rangle$ can be chosen as

$$|IMK\alpha\rangle = \frac{1}{\sqrt{2(1+\delta_{K0})}}\Big[|IMK\rangle+(-1)^I|IM-K\rangle\Big] \quad (K\geqslant 0), \tag{2}$$

where $|IMK\rangle$ is the Wigner D function and α denotes other quantum numbers. The angular momentum projections onto the 3-axis in the intrinsic frame and z-axis in the laboratory are denoted by K and M, respectively. Since the energy states are irrelevant to M, M is neglected in the following expressions.

The TRM Hamiltonian (1) can be written as

$$\hat{H} = \Big[\frac{1}{2}(A_1+A_2)(\hat{I}^2-\hat{I}_3^2)+A_3\hat{I}_3^2\Big] + \frac{1}{4}(A_1-A_2)(\hat{I}_+^2+\hat{I}_-^2), \tag{3}$$

with the raising and lowering operators $\hat{I}_\pm=\hat{I}_1\pm\mathrm{i}\hat{I}_2$. The first term of the Hamiltonian is diagonal while the second term only includes non-diagonal elements. The diagonal elements of $\hat{H}$ are

$$\langle IK|\hat{H}|IK\rangle=\frac{1}{2}(A_1+A_2)[I(I+1)-K^2]+A_3K^2. \tag{4}$$

The second term of Eq. (3) will cause a mixture of different states with $\Delta K=\pm 2$ and the corresponding matrix elements are

$$\langle IK|\hat{H}|IK\pm 2\rangle = \frac{1}{4}(A_1-A_2)\sqrt{(I\mp K)(I\pm K+1)(I\mp K-1)(I\pm K+2)}. \tag{5}$$

The energy eigenvalues and eigenstates for a given spin I can be obtained by solving the eigen equation.

The reduced electric quadrupole (E2) transition probability is defined as [1]

$$B(\mathrm{E2},I\to I')=\sum_{\mu KK'}|\langle I'K'|\hat{\mathcal{M}}_{2\mu}^E|IK\rangle|^2. \tag{6}$$

using the quadrupole transition operator

$$\hat{\mathcal{M}}_{2\mu}^E=\sqrt{\frac{5}{16\pi}}\hat{Q}_{2\mu}, \tag{7}$$

of which the laboratory electric quadrupole tensor operator $\hat{Q}_{2\mu}$ is associated with the intrinsic ones via the Wigner D function

$$\hat{Q}_{2\mu}=\mathcal{D}^{2*}_{\mu 0}\hat{Q}'_{20}+(\mathcal{D}^{2*}_{\mu 2}+\mathcal{D}^{2*}_{\mu -2})\hat{Q}'_{22}=\sum_\nu \mathcal{D}^{2*}_{\mu\nu}\hat{Q}'_{2\nu}. \tag{8}$$

The intrinsic quadrupole tensor operators are expressed by the intrinsic quadrupole Q and triaxial deformation γ as

$$Q'_{20}=Q\cos\gamma, \quad Q'_{22}=\frac{1}{\sqrt{2}}Q\sin\gamma. \tag{9}$$

With the solutions of the TRM, one can also investigate the angular momentum geometry. The expectation values of the squared angular momentum components for the total nucleus are calculated as $I_k=\sqrt{\langle\hat{I}_k^2\rangle}$ (k=1, 2, 3). From the obtained angular momenta, the orientation of the total angular momentum, depicted by the polar angle θ and azimuth angle φ, can be extracted by

$$I_1=J\sin\theta\cos\varphi,\quad I_2=J\sin\theta\sin\varphi,\quad I_3=J\cos\theta, \tag{10}$$

namely,

$$\theta=\cos^{-1}\left(\frac{I_3}{J}\right),\quad \varphi=\tan^{-1}\left(\frac{I_2}{I_1}\right), \tag{11}$$

where J is the length of the total angular momentum $J=\sqrt{I(I+1)}$.

2.2 Approximate analytic expressions

To find the analytic expressions for wobbling excitations, Bohr and Mottelson introduced the harmonic approximation for angular momentum operators [1]. Taking the 3-axis as the axis of the largest MOI, in the HA, the third component of angular momentum $\hat{I}_3$ is approximated as a constant value I, and the angular momentum raising and lowering operators are expressed in terms of boson creation and annihilation operators

$$\hat{I}_+=\sqrt{2I}\hat{a}^\dagger,\quad \hat{I}_-=\sqrt{2I}\hat{a}, \tag{12}$$

with $[\hat{a},\hat{a}^\dagger]\approx1$. With this assumption, the energy spectra can be expressed as the sum of two parts [1]

$$E(n,I)=A_3I(I+1)+\left(n+\frac{1}{2}\right)\hbar\omega. \tag{13}$$

The first part is the rotation energy with respect to the rotational axis with spin I and the second part is a harmonic oscillation energy, i.e., wobbling energy, with wobbling phonon number n. In detail, the wobbling phonon number n characterizes the wobbling motion of the axes with respect to the direction of I and the wobbling frequency $\hbar\omega$ is determined by the MOI as [1]

$$\hbar\omega=\sqrt{\alpha^2-\beta^2}I=2I\sqrt{(A_2-A_3)(A_1-A_3)}, \tag{14}$$

with

$$\alpha=A_2+A_1-2A_3,\quad \beta=A_2-A_1. \tag{15}$$

Since the wobbling motion has the characteristics of a harmonic oscillator, one can extract the "kinetic" and "potential" terms by combining the wobbling boson creation and annihilation operators. They are respectively written as $(A_2-A_3)I_2^2$ and $(A_1-A_3)I_1^2$ when the nucleus rotates around the 3-axis.

With the HA, the intraband B(E2) transition probabilities are approximated as [1]

$$B(\mathrm{E2};n,I\to n,I-2)\approx\frac{5}{16\pi}Q_{22}'^2, \tag{16}$$

and the interband ones [1]

$$B(\mathrm{E2};n,I\to n+1,I-1)=\frac{5}{16\pi}\frac{n+1}{I}\left(\sqrt{3}Q'_{20}y+\sqrt{2}Q'_{22}x\right)^2, \tag{17}$$

and

$$B(\mathrm{E2};n,I\to n-1,I-1)=\frac{5}{16\pi}\frac{n}{I}\left(\sqrt{3}Q'_{20}x+\sqrt{2}Q'_{22}y\right)^2, \tag{18}$$

where the coefficients are defined as

$$\left.\begin{matrix}x\\y\end{matrix}\right\}=\sqrt{\frac{1}{2}\left(\frac{\alpha}{\sqrt{\alpha^2-\beta^2}}\pm1\right)}. \tag{19}$$

The definitions for the intrinsic quadrupole moments Q'_{20} and Q'_{22} are the same as Eq. (9).

In the HA method, the angular momenta are expanded by boson operators only in zeroth order. Tanabe and Sugawara-Tanabe further applied the HP transformation [32] to the TRM Hamiltonian [27, 28]. The HP transformation expresses the angular momentum operators in terms of boson creation and annihilation operators as

$$\begin{aligned}\hat{I}_3&=I-\hat{n},\\ \hat{I}_+&=\hat{a}^\dagger\sqrt{2I}\sqrt{1-\frac{\hat{n}}{2I}},\\ \hat{I}_-&=\sqrt{2I}\sqrt{1-\frac{\hat{n}}{2I}}\hat{a}.\end{aligned} \tag{20}$$

with $\hat{n}=\hat{a}^\dagger\hat{a}$. When $I\gg1$ and $\hat{n}$ is small, the square roots $\sqrt{1-\frac{\hat{n}}{2I}}$ can be expanded as Taylor series with respect to $\hat{n}=0$. If the expansion is in zeroth order, the HP transformation degenerates to the HA method (12). By taking into account the effect of the next-to-leading order term, the wobbling energy spectra are finally given by [27, 28]

$$E(n,I)=A_3I(I+1)+\left(I\sqrt{\alpha^2-\beta^2}+\frac{1}{2}\sqrt{\alpha^2-\beta^2}-\frac{\alpha}{2}\right)\left(n+\frac{1}{2}\right)-\frac{\alpha}{2}n^2. \tag{21}$$

The definitions of α and β can be found in Eq. (15).

3 Numerical details

In the following, the wobbling motion for a triaxial rotor with $A_1=2A_2=6A_3=0.06$ MeV/$\hbar^2$ is discussed. The MOI values of the three axes are thus $\mathcal{J}_1=8.33$ $\hbar^2$/MeV, $\mathcal{J}_2=16.66$ $\hbar^2$/MeV, and $\mathcal{J}_3=50.00$ $\hbar^2$/MeV. That is,

the largest and the smallest MOI axes are the 3-axis and 1-axis respectively. The assumption for the MOI is the same as Ref. [16]. With this MOI assignment, the validity of the harmonic approximation exists in the spin region $I \gg (2\hat{n}+1)\frac{A_2+A_1-2A_3}{2\sqrt{A_1-A_3}\sqrt{A_2-A_3}} \approx (2\hat{n}+1)$ [1]. For the B(E2) calculations, the intrinsic quadrupole moment Q_0 is taken as $\sqrt{16\pi}$eb and the triaxial deformation parameter is assumed to be $\gamma=30^\circ$.

4 Results and discussion

In the following, we first present the energy spectra and electromagnetic transition probabilities obtained by the TRM and compare them with those from the HA and HP methods. The angular momentum evolution picture will then be discussed in detail. Finally, the microscopic understanding of this evolution will be shown.

4.1 Energy spectra

In Fig. 1, the energy spectra as functions of spin I calculated by the TRM are shown. The states with signatures $\alpha=0$ and $\alpha=1$ are plotted by full and empty dots respectively. The approximate quantum number n ($n=0,\ 1,\ 2,\ \cdots$) is introduced to label the energy states in order of their energies, and the energy for each state is denoted by $E(n,I)$. Since a triaxial nucleus possesses D_2 symmetry, the energy spectra are restricted to states with $(-1)^n=(-1)^I$ [1], i.e., only even spins appear for even-n states while only odd spins appear for odd-n states. Thus, there are $I/2+1$ states for a given even spin I, while there are $(I-1)/2$ states for odd spin I.

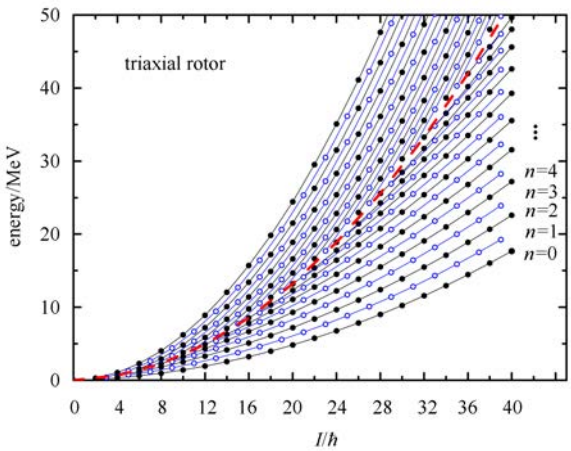

Fig. 1. (color online) Energy spectra as functions of spin I for a triaxial rotor with $A_1=2A_2=6A_3=0.06$ MeV/$\hbar^2$ calculated by TRM. The full dots belong to the states with signature $\alpha=0$, while empty dots to signature $\alpha=1$. The approximate quantum number n (n=0, 1, 2, $\cdots$) is introduced to label the energy states in accordance with the increasing order of their energies. A similar figure can be found in Ref. [16].

The obtained energy spectra can be divided into two different groups, which are distinguished by the manners of linking. One of them consists of the lines linking states with the same n for n-small bands. With increasing spin, the energy spacing between neighboring lines become more and more equivalent. This is the classical wobbling regime, which corresponds to the wobbling motion around the axis with the largest MOI (i.e. the 3-axis). The other group of spectra consists of the lines linking states with the same I–n for n-large bands, which corresponds to the wobbling motion around the axis with the smallest MOI (i.e. the 1-axis). Between these two groups is the separatrix region, which has the energy of unstable uniform rotation about the axis with the intermediate MOI.

To examine the accuracy of the HA (13) and HP (21) formulas, the energy spectra and wobbling energies as functions of spin for the four lowest wobbling bands obtained are compared with the exact solutions given by the TRM and shown in Fig. 2. The wobbling energies, defined as the energy differences between the excited states and the yrast state, are extracted from the obtained energy spectra and for a given spin I are calculated as

$$E_{\rm wob}=E(n,I)-E(0,I) \tag{22}$$

for even I, and

$$E_{\rm wob}=E(n,I)-\frac{1}{2}[E(0,I-1)+E(0,I+1)] \tag{23}$$

for odd I.

It can be seen that the wobbling energies obtained by the three methods all increase with the spin. This phenomenon can be microscopically understood from the fact that the stiffness of the collective potential increases with spin [26]. Both the HA and HP methods can reproduce the TRM results for both energy spectra and wobbling energies over the whole spin range for small n wobbling bands. However, with the increasing of n, the HA gradually deviates from the TRM results. For example, the HA results are larger than the TRM results by about 150 keV for the n=2 wobbling band and by about 350 keV for the n=3 wobbling band. This indicates that the wobbling motion can no longer be characterized as a good harmonic oscillator if n becomes too large and the anharmonicity of wobbling motions begins to play an important role [6, 33, 34]. The occurrence of anharmonicity can be described by taking into account the higher order terms in the expansion of angular momenta. This statement is supported by the fact that the HP formula reproduces the exact solutions perfectly. The energy differences between the HP and TRM results are less than 30 keV even for the n=3 wobbling band.

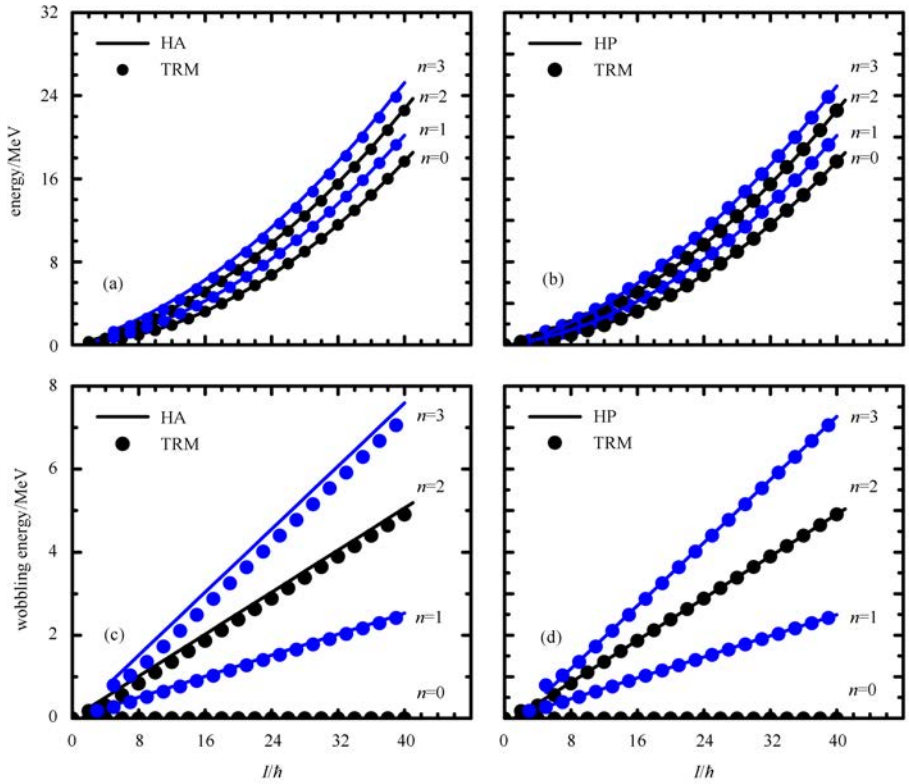

Fig. 2. (color online) The energy spectra and wobbling energies for the four lowest wobbling bands calculated by TRM are compared with those obtained by the HA (a, c) and HP (b, d) formulas.

To investigate the effects of the high order terms quantitatively, the energy differences obtained by the HA and HP methods are calculated as

$$E_{\rm HA}(n,I)-E_{\rm HP}(n,I)=\frac{\alpha}{2}n^2-\left(\frac{1}{2}\sqrt{\alpha^2-\beta^2}-\frac{\alpha}{2}\right)\left(n+\frac{1}{2}\right). \tag{24}$$

This depends on wobbling phonon number n, while it is independent of spin, i.e. the role played by the next-to-leading term is different for different n while it is the same for different spin. It is obvious that with the increase of n, the energy difference between HP and HA becomes larger, which indicates that the high order terms become more important and cause the wobbling motion to deviate from harmonic oscillator behavior.

4.2 Quadrupole transition probability

In Fig. 3, the intraband and interband B(E2) values for the $n=0$, $n=1$, and $n=2$ bands calculated by the TRM are shown in comparison with those calculated by the HA formula [1]. For the intraband B(E2) values, the HA results given by Eq. (16) are constants, which are independent of spin I and wobbling phonon number n. However, as shown in Fig. 3, the TRM results depend not only on spin but also on the wobbling phonon number. For each wobbling band n, the intraband B(E2) values gradually increase with increasing spin and finally come close to the HA results at very high spin. For a given spin, with the increase of n, the corresponding B(E2) values decrease. Therefore, one can conclude that the HA formula is a good approximation only at very high spin and small n. This is expected since the approximation for vector addition coefficients in the E2 matrix elements, which is valid only at very high spin, has been adopted when deriving the HA formula [1].

For interband B(E2) values, the HA results exhibit a decreasing trend with respect to spin for a given n and increasing trend with respect to n for a given spin, which are determined by the factor n/I in the HA formulas (17) and (18). It can be further seen that the $B(\mathrm{E2};n,I\rightarrow n+1,I-1)$ values are smaller than the $B(\mathrm{E2};n+1,I\rightarrow n,I-1)$ values over the whole spin region since the bracketed terms in Eq. (17) are smaller than the bracketed terms in Eq. (18). For the TRM results, the decreasing trends with respect to spin can also be found in the high spin region, while in the low spin region, contrary to the HA results, an increasing trend is shown for the interband transition between the $n=1$ and $n=2$ bands. For example, the $B(\mathrm{E2};2,I\rightarrow 1,I-1)$ values increase rapidly with spin at $I\leqslant 10\hbar$.

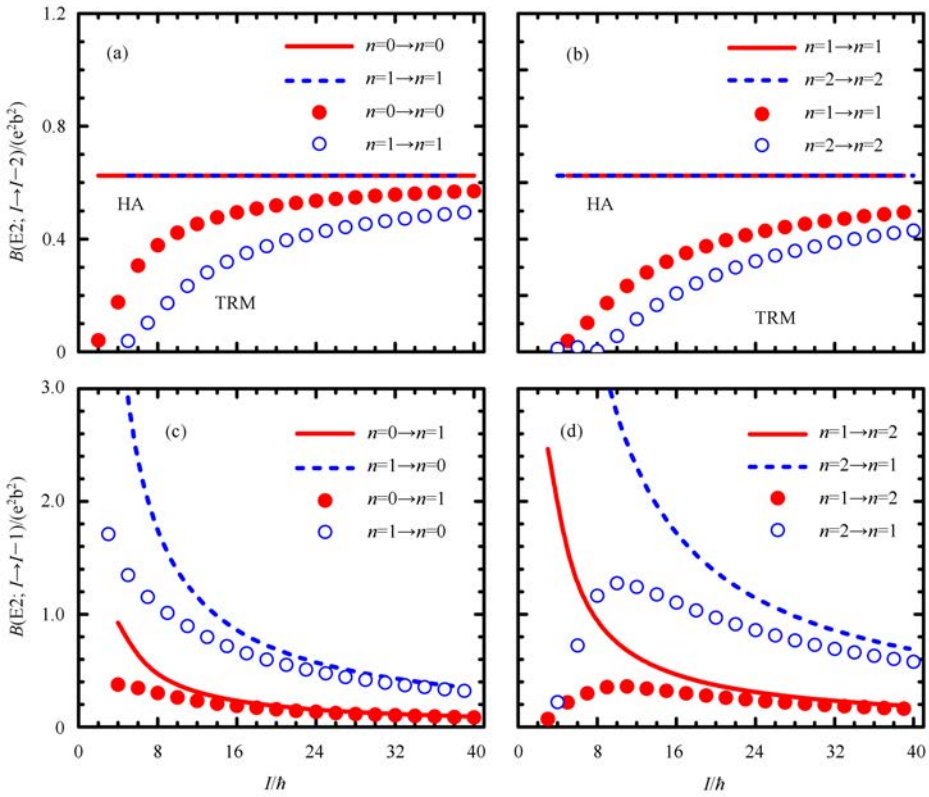

Fig. 3. (color online) The intraband and interband B(E2) values for $n=0$, 1 (a, c) and $n=1$, 2 (b, d) bands calculated by the TRM in comparison with those from the HA formula [1].

It can be seen that the HA results in general overestimate the TRM results. In particular, this overestimation becomes larger with the increase of the wobbling phonon number n. For a given n, the TRM results gradually come close to the HA results as spin increases. Therefore, similar to the case of intraband transition probabilities, the interband transition probabilities obtained by the HA formula are good approximations for those obtained by the TRM only in the high spin region and for small n.

Comparing the interband transition with the intraband transition, it is seen that the strength of the interband $B(\mathrm{E2};n,I\rightarrow n\pm1,I-1)$ is smaller than that of the intraband $B(\mathrm{E2};n,I\rightarrow n,I-2)$ without changing the wobbling phonon number n in the high spin region, by a factor of order $\frac{n}{I}$, which represents the square of the amplitude of the wobbling motion [1]. This is an expected feature of the wobbling bands, which corresponds to a sequence of one-dimensional rotational trajectories with a strong E2 transition along the trajectories and much weaker transitions connecting the different trajectories [1].

4.3 Angular momentum

To understand the wobbling geometry picture, it is necessary to investigate the evolutionary picture of angular momentum components with respect to spin I and wobbling phonon number n. In Fig. 4, the angular momentum components I_k as functions of spin for the n=0–5 bands calculated by the TRM are shown. For the n=0 band, all of the three components of the angular momentum I_k of the triaxial rotor gradually increase as the spin increases. However, the roles they play are quite different. The angular momentum favors alignment along the 3-axis with the largest MOI to obtain the lowest energy. The value of I_3 is nearly equal to I. The contributions from the other two axes to the total angular momentum are thus very small due to the conservation of angular momentum

$$I_1^2+I_2^2+I_3^2=J^2=I(I+1). \tag{25}$$

It is worth pointing out that the angular momentum along the 3-axis and the other two axes (1-, 2-axis) respectively contribute to the rotational energy and the zero energy of the wobbling motion for the wobbling energy spectra.

With the increase of the wobbling phonon number n, the angular momentum shows a tendency to gradually deviate from the 3-axis. The value of I_3 is nearly equal to I–n at large spin region. Meanwhile, the values of the 1- and 2- components of the angular momentum become

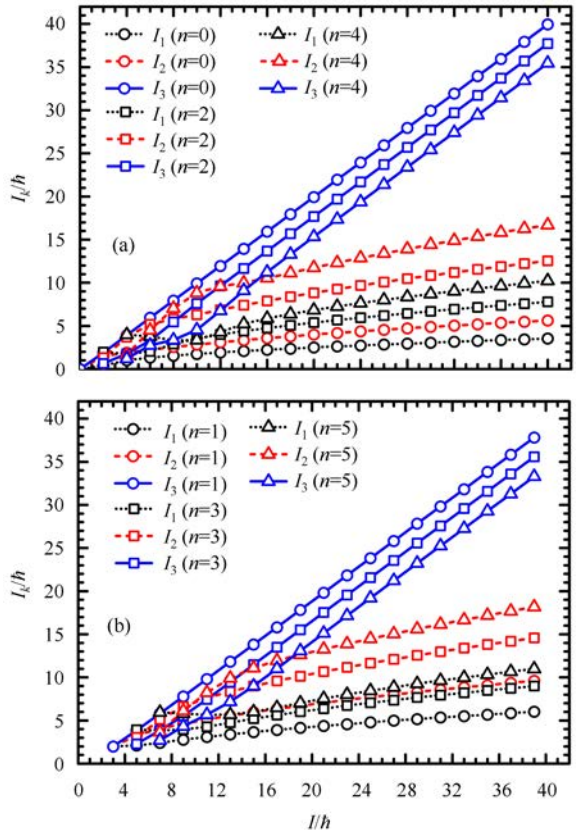

Fig. 4. (color online) The root mean square components along the 1, 2, and 3 axis of the total nucleus $I_k=\sqrt{\langle\hat{I}_k^2\rangle}$ calculated as functions of spin I by TRM for (a) even n wobbling bands (n=0, 2, 4) and (b) odd n wobbling bands (n=1, 3, 5).

larger and larger, which indicates that the wobbling motion plays a more and more important role.

It should be noted that when the wobbling phonon number n is larger than 2, the three components of the angular momentum will present a strong competitive behavior. This gives a clear picture that with the increase of spin the maximal component of the angular momentum changes from I_1 to I_2 and finally to I_3. Here, the evolution of the angular momentum with spin for the n=4 band will be taken as an example to illustrate this picture. At spin I=4$\hbar$, the n=4 state is the largest energy state, as shown in Fig. 1, and the angular momentum aligns mainly along the 1-axis, which corresponds to the wobbling motion along the axis with the smallest MOI. In the spin region $6\leqslant I\leqslant 14\hbar$, the angular momentum turns to align mainly along the 2-axis with intermediate MOI. It can be seen from Fig. 1 that these states lie around the separatrix region. When spin $I>16\hbar$, the angular momentum finally aligns mainly along the 3-axis, which corresponds to the wobbling motion along the axis with the largest MOI. As shown in Fig. 1, these states are beneath the separatrix line and move further away from it as the spin increases.

It has been emphasized that complex competition exists among the three components of angular momenta with spin I in the same n wobbling bands. It is also interesting to investigate the evolution picture with respect to the wobbling phonon number for a given spin I. Therefore, in Fig. 5, the root mean square components along the 1, 2, and 3 axis of the total angular momentum I_k calculated by the TRM as functions of the wobbling phonon number n are shown respectively for $I=10\hbar$ (Fig. 5(a)) and I=30$\hbar$ (Fig. 5(b)).

For I=10$\hbar$, in general, the I_3 decreases while the I_1 increases as the wobbling phonon number n increases, which indicates that the angular momentum generally has a tendency to move away from the 3-axis at small n and towards the 1-axis at large n. However, I_3 shows a slightly increasing behavior when n increases from 4 to 6. The angular momentum of the n=6 state is closer to the 3-axis than that of the n=4 state, although the difference between them is small. This indicates that the angular momentum does not always steadily deviate from the 3-axis with increasing n. It is further noted that I_1 also exhibits abnormal behavior. When n increases from 2 to 4, it decreases by about 0.2$\hbar$. Thereafter, it increases linearly with increasing n. Differing from the behaviors of I_1 and I_3, I_2 first increases, for $n\leqslant 4$, and then decreases. Therefore, the strong competition among the three components of the angular momentum is clearly presented. When n=0 and 2, I_3 is largest and $I_2>I_1$. This region is labeled as (III) in the figure. When n=4 and 6, I_2 becomes the largest component and I_1 and I_3 compete with each other. This region is labeled as (II). Finally, when n increases to 8 and 10, I_1 begins to play the main role while I_3 becomes the smallest. Correspondingly, this region is labeled as (I). For I=30$\hbar$, the evolution behaviors of these three components of angular momentum are very similar to those for I=10$\hbar$. The abnormal behaviors exhibited by I_3 and I_1 happen at n=14, 16 and n=10,12, while I_2 reaches its maximal value at n=14. In addition, with increasing n, the three components of angular momentum present a strong competitive behavior. Similar to the case of I=10$\hbar$, (III), (II), and (I) are labeled according to the maximal components of the angular momentum.

It can thus be concluded that with the increase of the wobbling phonon number n for a certain spin I, the simple triaxial rotor undergoes three different kinds of behavior regimes, labeled as regions (III), (II), and (I) in Fig. 5. In region (III), I_3 is the largest, corresponding to the wobbling motion around the 3-axis, which has the largest MOI. This is further supported by the nearly equivalent contributions of the "kinetic" term $(A_2-A_3)I_2^2$ and "potential" term $(A_1-A_3)I_1^2$ in this region, as shown

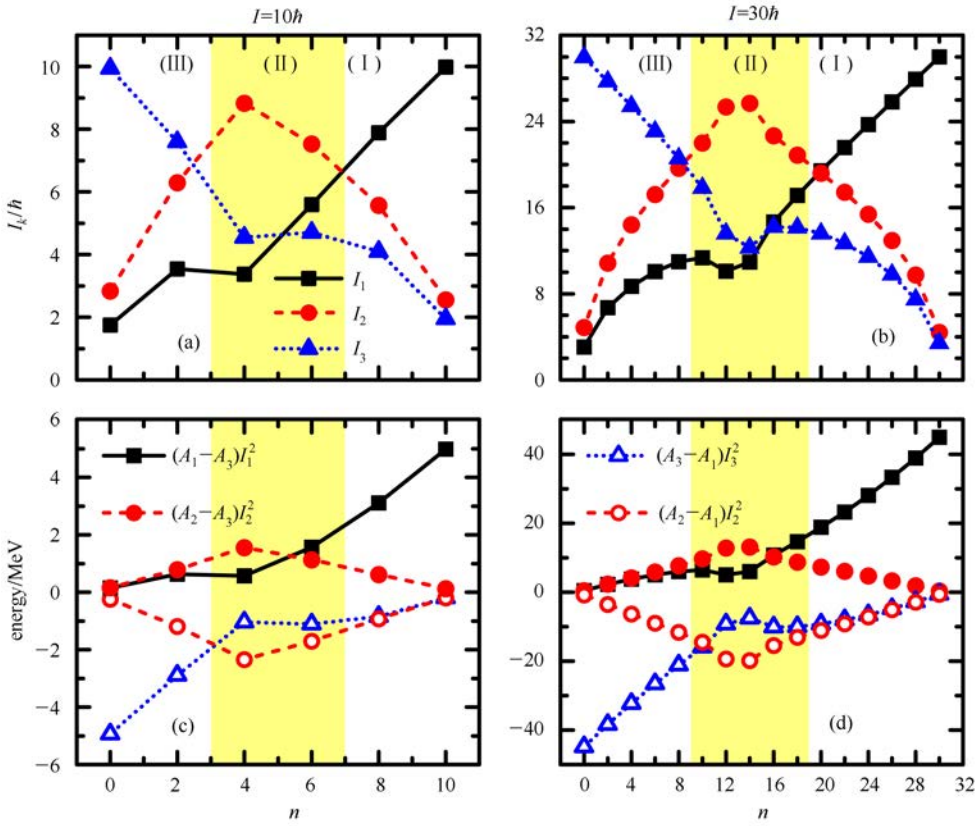

Fig. 5. (color online) The root mean square components along the 1, 2, and 3 axis of the total angular momentum $I_k=\sqrt{\langle\hat{I}_k^2\rangle}$ calculated by the TRM and their corresponding contributions to the "kinetic" and "potential" terms of wobbling energy as functions of the wobbling phonon number n for $I=10\hbar$ (a, c) and $I=30\hbar$ (b, d).

in Figs. 5(c) and (d). In addition, in this region, I_3 is approximately linear to n with $I_3\approx I-n$. In region (Ⅰ), however, I_1 is the largest, which corresponds to the wobbling motion around the 1-axis, which has the smallest MOI. Similarly, this is also supported by the equivalent contributions of the "kinetic" term $(A_3-A_1)I_3^2$ and "potential" term $(A_2-A_1)I_2^2$ in this region, as shown in Figs. 5(c) and (d). Similar to I_3, I_1 is also approximately linear with n with $I_1\approx n$ for even spin and $I_1\approx n+1$ for odd spin. In the transitional region (Ⅱ), which corresponds to the separatrix region in Fig. 1, I_1, I_2 and I_3 exhibit a completely different behavior from that in the other two regions and fierce competition among the three components of angular momentum is clearly shown. This competition might be associated with the phenomenon, as shown in Fig. 1, that the energy in this region increases slowly compared with that in the other two regions as n increases. In addition, although I_2 is the largest, there is no wobbling motion around the 2-axis, which has intermediate MOI, since the "kinetic" term $(A_1-A_2)I_1^2$ is positive $(A_1>A_2)$ while the "potential" term $(A_3-A_2)I_3^2$ negative $(A_3<A_2)$. This conclusion is consistent with that obtained by the tops-on-top model [35].

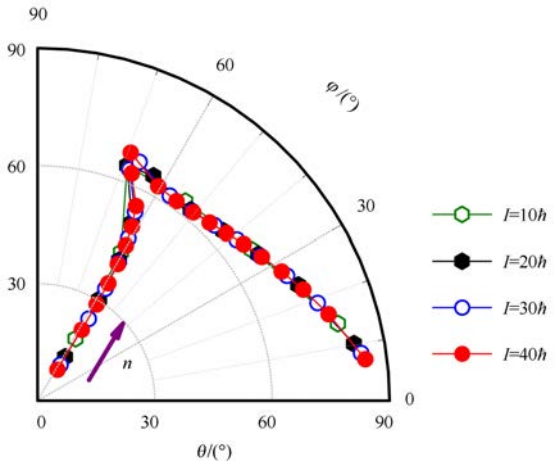

Fig. 6. (color online) The calculated orientation of the total angular momentum, depicted by the polar angle θ and azimuth angle φ, as a function of the wobbling phonon number n for $I=10$, 20, 30 and $40\hbar$. The θ and φ are shown in a polar coordinate system, in which θ is the radial coordinate while φ is the angular coordinate. The arrow indicates the increasing direction of the wobbling phonon number.

In order to further clarify the angular momentum evolution, in Fig. 6, the orientation of the total angular momentum, depicted by the polar angle θ (11) and azimuth angle φ (11), is illustrated as a function of wobbling phonon number n for I=10, 20, 30 and 40$\hbar$.

It is clearly seen that the series of points with the wobbling phonon number n lies on the same line for all spin I, which indicates that no matter what the spin I is, the orientations of the angular momentum vectors are along the same evolution track with increasing n. When n is small, φ is almost invariable while θ increases as n increases, which suggests that the angular momentum vector lies almost in the same plane $\varphi\approx 60^\circ$ but gradually deviates from the 3-axis as n increases. The reason for angular momentum being in the plane $\varphi\approx 60^\circ$ can be understood according to the "kinetic" and "potential" terms in the TRM Hamiltonian as shown in Figs. 5(c) and (d). Since the "kinetic" term $(A_2-A_3)I_2^2$ and "potential" term $(A_1-A_3)I_1^2$ are almost equivalent for small n, this indicates that $\varphi=\tan^{-1}\left(\frac{I_2}{I_1}\right)$ approximates as $\tan^{-1}\sqrt{\frac{A_2-A_3}{A_1-A_3}}$. Thus φ is independent of θ but determined by the three MOIs at small n. According to this formula, one can obtain $\varphi\approx 60^\circ$ in the present system under discussion. It is noted that these energy states correspond to the wobbling motion along the 3-axis and mainly lie in region (III) shown in Fig. 5. As n increases, both θ and φ increase, which suggests that the angular momentum not only continues to deviate from the 3-axis, but also starts moving to the 2-axis. However, the trend of increasing φ is not incessant but is interrupted at a critical point. This critical point corresponds to the maximal values of I_2, as shown in Fig. 5(a) and (b). After that, φ, together with θ, begins to decrease. This indicates that the angular momentum moves to the 1-axis, and at the same time also moves slightly to the 3-axis. The points around the critical point correspond to the transition region (II) shown in Fig. 5. After crossing this region, φ decreases while θ increases with increasing n, moving to region (I) shown in Fig. 5. Similar to the cases of small n, according to Figs. 5(c) and (d), in this region $\frac{I_3}{I_2}=\sqrt{\frac{A_3-A_1}{A_2-A_1}}$, which implies that the angular momentum vectors for large n also lie in the same plane, perpendicular to the 2-3 plane.

According to the above discussion, the evolution track of angular momenta with respect to the wobbling phonon number presented in Fig. 6 is determined only by the three MOIs of the triaxial rotor. As already pointed out above, the evolution track is unique and independent of spin. From this point of view, this evolution track may be regarded as a characteristic feature for a rotating triaxial rotor. Along this evolution track, the triaxial rotor changes its rotation along the axis with the largest MOI to the axis with the smallest MOI.

4.4 *K*-distribution

In the above, the angular momentum geometry of wobbling motion for the triaxial rotor is investigated via the expectation values of the three components of the angular momentum. It is interesting to further investigate the angular momentum geometry pictures from a microscopic perspective by the obtained wave functions. In the TRM, the wave functions can be directly reflected by the so called K-distributions, i.e., the probability distributions of the projections of total angular momentum on the 1-, 2- and 3- axes. In the literature, using the PRM, such K-distributions have been extensively applied to study the angular momentum geometry of the nuclear chiral modes in triaxial nuclei [36–39].

In the following, the K-distributions for the n=0, 2, 4 states with I=10 and 30$\hbar$ and n=1, 3, 5 states with I=9 and 29$\hbar$, shown in Fig. 7, are taken as examples to microscopically understand the angular momentum geometry.

It can be seen that for $n=0$ states, the maximal probability for the 3-axis appears at $K_3=I$ for both I=10 and 30$\hbar$, while the probabilities for the other K_3 values almost vanish. This is expected since the angular momentum is mainly along the 3-axis, as shown in Fig. 5. The probability distributions with respect to the 2- and 1-axis have peaks near $K_2=2\hbar$ and $K_1=2\hbar$ for both $I=10$ and 30$\hbar$. The reason why these peaks do not appear at $K_2=0$ and $K_1=0$ is attributed to the nature of three-dimensional rotation of the triaxial rotor, where the three angular momentum components I_k all have contributions to the total spin. As the MOI of the 2-axis is larger than that of the 1-axis, the angular momentum is closer to the 2-3 plane than the 1-3 plane. Thus the tunneling of angular momentum with respect to the 2-3 plane is easier than for the 1-3 plane. This phenomenon can be reflected by the probability of K_1=0 being larger than that of K_2=0.

As n increases, for large spin, e.g., $I=29$ and 30$\hbar$, the peak of the probability on the 3-axis moves away from $K=I$ to $K=I-n$, corresponding to a deviation from the 3-axis, which suggests that the distributions from I_1 and I_2 become more important. Meanwhile, for K_1 and K_2, more peaks appear and it is expected that the number of peaks is $n+1$ if the K-distributions are plotted also for negative K values. It is noted that for the even n and odd n states, the probabilities on the 1- and 2- axis are respectively nonzero and zero at $K=0$, which indicates that their corresponding wave functions are symmetric and antisymmetric in the projections on the 1- and 2- axis. We should bear in mind that all the states presented for large spin lie in region (III), where

the wobbling motions happen along the axis with largest MOI. Once the states lying in the other two regions are involved, the K-distributions would exhibit a different behavior. This can be seen for small spin when n is not too large, e.g., the $n=4$ state with $I=10\hbar$, which lies in region (Ⅱ). Therefore, further investigation is necessary for the evolution of the K-distribution with respect to the wobbling phonon number n.

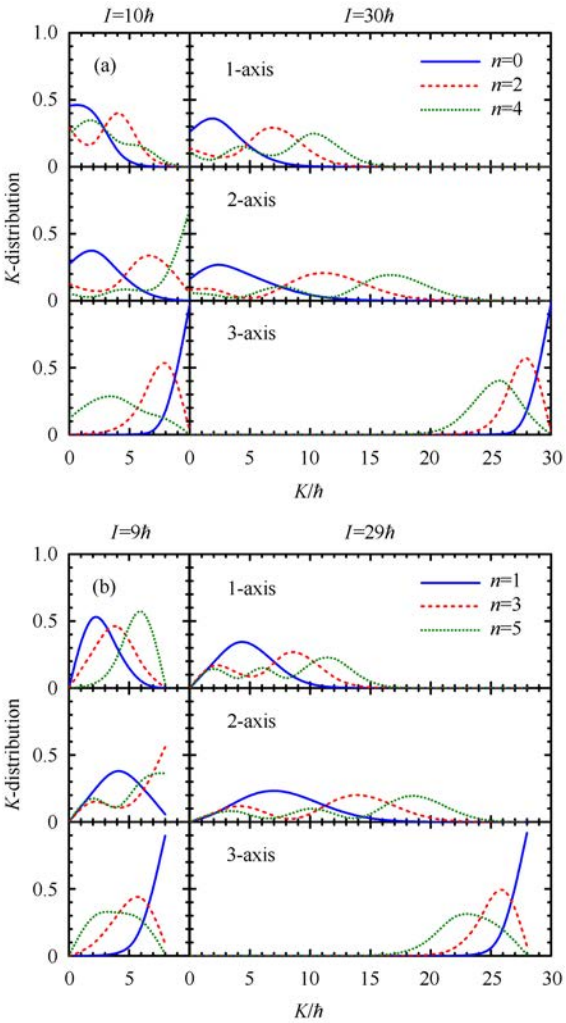

Fig. 7. (color online) The probability distributions for projections of total angular momentum on the 1-, 2- and 3- axis in the TRM for (a) $n=0$, 2, 4 states with $I=10$ and $30\hbar$ and (b) $n=1$, 3, 5 states with $I=9$ and $29\hbar$.

In Fig. 8, the K-distributions for the $n=0$–10 states are shown. For $n=4$, the probability for $K_2=I=10\hbar$ is much larger than that for other K_2. Compared with region (Ⅱ) in Fig. 5, this corresponds to the situation where I_2 is the largest angular momentum component and the angular momentum mainly aligns along the 2-axis. In this case, the probability distributions with respect to the 1- and 3-axis have peaks near $K_1=2\hbar$ and $K_3=4\hbar$. As n increases, the peak of the probability on the 1-axis gradually moves towards $K_1=I$ and the peaks for each n state appear nearly at $K_1=n$, which indicates a trend of the angular momentum moving to the 1-axis. This evolution picture is consistent with the evolution picture of angular momentum shown in Fig. 5.

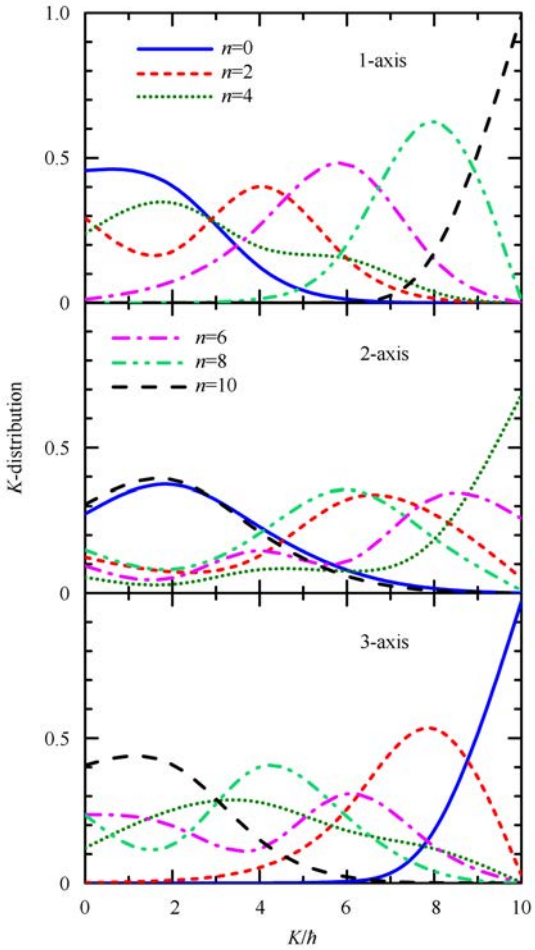

Fig. 8. (color online) The probability distributions for projections of total angular momentum on the 1-, 2-, and 3-axis in the TRM for $n=0$–10 states with $I=10\hbar$.

It is interesting to note that the K-distribution on the 1-axis and 3-axis for the $n=8$ and $n=10$ states are respectively similar to those distributions on the 3-axis and 1-axis for the $n=2$ and $n=0$ states. Moreover, the K-distribution on the 2-axis for $n=0$ and $n=10$ states as well as $n=2$ and $n=8$ states are also very similar. These similar behaviors are justified since the wobbling motions happen along both the 1- and 3- axis. These similarities between the pictures for wobbling motion around the 1-axis and 3-axis are consistent with the pictures of the components of angular momentum shown in Fig. 5.

5 Summary

In summary, a simple triaxial rotor is taken as an example to illustrate the picture of wobbling motion by exactly solving the TRM Hamiltonian. The obtained energy spectra and reduced quadrupole transition probabilities are compared to those approximate analytic solutions by the HA [1] and HP [27–29] methods to evaluate the accuracy of the analytic methods. It is found that only the low lying wobbling bands can be well described by the analytic HA solutions. By taking the higher order terms into account, the HP method improves the HA descriptions for the energy spectra.

The evolution of angular momentum geometry with respect to the spin and the wobbling phonon number are investigated. It is confirmed that with the increase of the wobbling phonon number, the triaxial rotor changes its rotation along the axis with the largest MOI to the axis with the smallest MOI. There is a competitive process among the three angular momentum components in the separatrix region, in which the angular momentum mainly aligns along the axis with intermediate MOI. Nevertheless, a specific track that can be used to depict the motion of a triaxial rotating nuclei at any spin is found along the evolutionary process. This evolutionary track may be regarded as a fingerprint of the triaxial rotor. The K-distribution further corroborates the evolution picture of the angular momentum.

For added perspective, it is interesting to investigate the angular momentum geometry of wobbling motion for odd-A nuclei, in particular the angular momentum geometry of longitudinal and transverse wobblers [16].

The authors are grateful to Prof. J. Meng, Prof. S. Q. Zhang, and H. Zhang for fruitful discussions and critical reading of the manuscript.

References

1 Bohr A, Mottelson B R. Nuclear Structure, Vol. II, Benjamin, New York, 1975
2 Frauendorf S, Meng J. Nucl. Phys. A, 1997, **617**: 131
3 Frauendorf S. Rev. Mod. Phys., 2001, **73**: 463
4 MENG J, ZHANG S Q. J. Phys. G: Nucl. Part. Phys., 2010, **37**: 064025
5 Ødegård S W, Hagemann G B, Jensen D R, Bergström M, Herskind B, Sletten G, Törmånen S, Wilson J N, Tjøm P O, Hamamoto I et al. Phys. Rev. Lett., 2001, **86**: 5866
6 Jensen D R, Hagemann G B, Hamamoto I, Ødegård S W, Herskind B, Sletten G, Wilson J N, Spohr K, Hübel H, Bringel P et al. Phys. Rev. Lett., 2002, **89**: 142503
7 Jensen D R, Hagemann G B, Hamamoto I, Ødegård S W, Bergstrom M, Herskind B, Sletten G, Tormanen S, Wilson J N, Tjom P O et al. Nucl. Phys. A, 2002, **703**: 3
8 Schönwaßer G, Hübel H, Hagemann G B, Bednarczyk P, Benzoni G, Bracco A, Bringel P, Chapman R, Curien D, Domscheit J et al. Phys. Lett. B, 2003, **552**: 9
9 Amro H, MA W C, Hagemann G B, Diamond R M, Domscheit J, Fallon P, Gorgen A, Herskind B, Hubel H, Jensen D R et al. Phys. Lett. B, 2003, **553**: 197
10 Hagemann G B. Eur. Phys. J. A, 2004, **20**: 183
11 Bringel P, Hagemann G, Hübel H, Al-khatib A, Bednarczyk P, Bürger A, Curien D, Gangopadhyay G, Herskind B, Jensen D et al. Eur. Phys. J. A, 2005, **24**: 167
12 Hartley D J, Janssens R V F, Riedinger L L, Riley M A, Aguilar A, Carpenter M P, Chiara C J, Chowdhury P, Darby I G, Garg U et al. Phys. Rev. C, 2009, **80**: 041304
13 ZHU S J, LUO Y X, Hamilton J H, Ramayya A V, CHE X L, JIANG Z, Hwang J K, Wood J L, Stoyer M A, Donangelo R et al. Int. J. Mod. Phys. E, 2009, **18**: 1717
14 Hamamoto I. Phys. Rev. C, 2002, **65**: 044305
15 Hamamoto I, Mottelson B R. Phys. Rev. C, 2003, **68**: 034312
16 Frauendorf S, Dönau F. Phys. Rev. C, 2014, **89**: 014322
17 Shimizu Y R, Matsuzaki M. Nucl. Phys. A, 1995, **588**: 559
18 Matsuzaki M, Shimizu Y R, Matsuyanagi K. Phys. Rev. C, 2002, **65**: 041303
19 Matsuzaki M, Shimizu Y R, Matsuyanagi K. Eur. Phys. J. A, 2003, **20**: 189
20 Matsuzaki M, Shimizu Y R, Matsuyanagi K. Phys. Rev. C, 2004, **69**: 034325
21 Matsuzaki M, Ohtsubo S. Phys. Rev. C, 2004, **69**: 064317
22 Shimizu Y R, Matsuzaki M, Matsuyanagi K. Phys. Rev. C, 2005, **72**: 014306
23 Shimizu Y R, Shoji T, Matsuzaki M. Phys. Rev. C, 2008, **77**: 024319
24 Shoji T, Shimizu Y R. Progr. Theor. Phys., 2009, **121**: 319
25 Oi M, Ansari A, Horibata T, Onishi N. Phys. Lett. B, 2000, **480**: 53
26 CHEN Q B, ZHANG S Q, ZHAO P W, MENG J. Phys. Rev. C, 2014, **90**: 044306
27 Tanabe K, Sugawara-Tanabe K. Phys. Lett. B, 1971, **34**: 575
28 Tanabe K, Sugawara-Tanabe K. Phys. Rev. C, 2006, **73**: 034305
29 Tanabe K, Sugawara-Tanabe K. Phys. Rev. C, 2008, **77**: 064318
30 Davydov A, Filippov G. Nuclear Physics, 1958, **8**: 237
31 ZENG J Y. Quantume Mechanics, Vol. II. Beijing: Science Press, 2007 (in Chinese)
32 Holstein T, Primakoff H. Phys. Rev., 1940, **58**: 1098
33 Oi M, Fletcher J. J. Phys. G, 2005, **31**: S1753
34 Oi M. Phys. Lett. B, 2006, **634**: 30
35 Sugawara-Tanabe K, Tanabe K, Yoshinaga N. Prog. Theor. Exp. Phys., 2014, 063D01
36 QI B, ZHANG S Q, MENG J, WANG S Y, Frauendorf S. Phys. Lett. B, 2009, **675**: 175
37 QI B, ZHANG S Q, WANG S Y, YAO J M, MENG J. Phys. Rev. C, 2009, **79**: 041302(R)
38 CHEN Q B, YAO J M, ZHANG S Q, QI B. Phys. Rev. C, 2010, **82**: 067302
39 QI B, ZHANG S Q, WANG S Y, MENG J, Koike T. Phys. Rev. C, 2011, **83**: 034303